Preparation of a Highly Porous Binderless Activated Carbon Monolith from Rubber Wood Sawdust by a Multi-Step Activation Process for Application in Supercapacitors

E. Taer[1,2], M. Deraman[1,], I. A. Talib[1], A. Awitdrus[1,2], S.A. Hashmi[3], A. A. Umar[4]*

[1] School of Applied Physics, Faculty of Science and Technology,
Universiti Kebangsaan Malaysia, 43600 Bangi, Selangor, Malaysia
[2] Department of Physics, University of Riau, 28293 Simpang Baru, Riau, Indonesia
[3] Departement of Physics and Astrophysics, University of Delhi, Delhi-110007, India
[4] Institute of Microengineering and Nanoelectronics, Universiti Kebangsaan Malaysia, 43600 Bangi, Selangor, Malaysia
[*]E-mail: madra@pkrisc.cc.ukm.my

Binderless activated carbon monoliths (ACMs) with high porosity that were prepared from self-adhesive pre-carbonized rubber wood sawdust were studied as electrodes for supercapacitors, focusing on the influence of activation time on the physical and electrochemical properties of the ACMs. The ACMs were activated under a flow of CO_2 gas at a rate of 0.5 liters per minute and at a temperature of 900 ^{o}C. Activation time varied from 1 to 6 hours and with a multi-step heating profile. The ACM was characterized physically (density, porosity, structure and surface morphology) and electrochemically (specific capacitance, equivalent series resistance, energy and power density). This study found that the combined effects from the length of activation time, binderless property and multi-step heating had the greatest influence on the physical and electrochemical properties of the ACM. The optimum ACM was activated for 5 hours and had a specific capacitance, equivalent series resistance, energy and power density of 138 F g^{-1}, 0.49 Ohm, 2.63 Wh kg^{-1} and 291 W kg^{-1}, respectively.

Keywords: Activated carbon monolith; Supercapacitor; Mesoporous carbon

1. INTRODUCTION

Fossil- and organic-based carbonaceous materials are amongst the most widely used starting or precursor materials for supercapacitor electrodes because they are relatively inexpensive and easy to fabricate. These electrode materials also have large specific surface areas, good electrical conductivity and excellent chemical stability [1, 2]. The carbonaceous materials extracted from biomass such as cassava peel waste [3], coffee bean waste [4], coffee shells [5], cherry stone [6], bamboo [7], fir woods

[8], banana fibers [9] and sugar cane bagasse [10] have been used as supercapacitor carbon electrodes; however, carbons from these precursors in general have been prepared in powder form. Therefore, to use them as electrodes in supercapacitors, they have to be formed into pellets or monolith structures. This process typically requires the addition of a binder to shape the carbon particles into the desired form. Several reports studying carbon electrodes without binders have been recently published [11-13]. These authors asserted that binderless electrodes have several advantages: (i) the binders occupy some of the pores and reduce electrolyte accessibility [14]; (ii) binders are non-conducting and therefore reduce the electrical conductivity of the electrodes [15]; and (iii) the use of binders adds both additional steps to the processing of the electrodes and an extra cost. In light of these points, the present study has chosen a pre-carbonized rubber wood sawdust (RWSD) as a precursor to produce porous carbon electrodes for application in a supercapacitor cell. The pre-carbonized RWSD is self-adhesive and can be shaped into green bodies in a monolithic form without adding any binder. The carbon monolith was activated by CO_2, and the porosity was optimized by varying the length of the activation time. To avoid forming cracks on the activated carbon monolith (ACM), a multi-step method of activation was introduced in which the total activation time was divided into several segments.

In most cases, the physicochemical properties of the carbon electrode (i.e., structure, porosity) were improved to meet the required specifications of each intended application through an activation process. In general, there are two types of activation methods: chemical and physical. Chemical activation consists of a single-step carbonization and activation by chemical agents (i.e., KOH, $ZnCl_2$ or H_3PO_4) at 400 to 800 ^{o}C [16]. For physical activation, carbonization of the carbon precursor is first carried out at ambient conditions and followed by activation at a higher temperature (i.e., 800-1000 ^{o}C) by activation agents (i.e., CO_2, air, steam or a mixture of these gases) [16]. In the present study, CO_2 activation was performed at 900 ^{o}C, as previously reported [17], with the activation time varying from 1 to 6 hours.

The ACM was characterized by X-ray diffraction (XRD), N_2-adsorption-desorption and field emission scanning electron microscopy (FESEM) to observe the effect of varying activation time on the physical properties of the ACM. These properties were used to interpret the electrochemical data of the supercapacitor cells fabricated using the ACMs as electrodes. Galvanostatic charge-discharge, cyclic voltammetry and electrochemical impedance spectroscopy (EIS) were used to evaluate electrochemical performance.

2. EXPERIMENTAL

2.1 Electrode preparation and cell fabrication

ACMs were prepared from the RWSD using our previously reported method [18]. Briefly, the RWSD was pre-carbonized at a low temperature (~280 ^{o}C), followed by a ball mill process for approximately 36 hours. Finally, the material was sieved to obtain a powder of self-adhesive carbon grain (SACG) with a particle size of less than 53 microns. Green monoliths (GM) of the SACG were

prepared in a mold (20 mm diameter) using 8 metric tons of compression force, then carbonized at ~600 $^{\circ}$C under a N_2 atmosphere to produce the carbon monolith. The carbon monolith was activated by CO_2 at ~900 °C with heating rate of 10 °C per minute. Several lengths of activation times were evaluated: 1, 2, 3, 4, 5 and 6 hours. The ACMs were identified as ACM1 to ACM6 in reference to activation times of 1 to 6 hours, respectively. The ACMs were then polished to the desired thicknesses and extensively washed with distilled water.

Activation for more than two hours created cracks in the samples. A multi-step activation method was implemented to avoid this cracking by dividing the total activation time into several segments according to the steps in Table 1. For each step, the furnace was allowed to cool to room temperature and was held at this temperature for 5 hours before proceeding to the next step.

Table 1. Step and duration selected in each step of the multi-step activation method.

Total Activation time (h)	Step 1 (h)	Step 2 (h)	Step 3 (h)
1	1	-	-
2	2	-	-
3	1	2	-
4	2	2	-
5	2	2	1
6	2	2	2

The symmetrical supercapacitor cells were fabricated to study the capacitive properties of the ACMs to be used as electrodes. The cell consists of two ACMs, two stainless steel current collectors (316-L stainless steel foils, Goodfellow Cambridge Ltd., England) and a liquid electrolyte between the ACM separated by a ring of Teflon spacer with a thickness of 0.1 mm. The diameter, thickness and weight of the ACM were 15 mm, 0.4 mm and 40-50 mg, respectively. Sulfuric acid (H_2SO_4, 1 M) served as the electrolyte.

2.2. Physical characterization

Density, porosity, structure and surface morphology were all evaluated in the present study. The dimension and weight of the ACM were measured to determine sample density. The porosity parameters of the ACM (i.e., Brunauer-Emmett-Teller (BET) surface area, micropore surface area, total pore volume and average pore diameter) were determined from the nitrogen adsorption data at -196 $^{\circ}$C using an accelerated surface area and porosimeter system (ASAP 2010, Micromeritics). The BET surface area was calculated from the isotherms using the BET equation [19]. In this experiment, the cross-sectional area of a nitrogen molecule was assumed to be 0.162 nm^2. The Dubinin-Radushkevich equation was used to calculate the micropore volume from which the micropore surface area was then determined [19]. The total pore volume was estimated to be the liquid volume of

adsorbate (N_2) at a relative pressure of 0.995. The structure of the ACM was elucidated by XRD. XRD patterns were obtained on a Bruker AXS D8 advance diffractometer that employed CuK_α radiation with a 2Θ range of 0 to 60°. The graphitic microcrystallite dimension (stack height = L_c, stack width = L_a) can be calculated from the XRD diffraction pattern using the Debye-Scherrer equation: $L_c = 0.90\lambda/\beta\cos(\Theta_{002})$ and $L_a = 1.94\lambda/\beta\cos(\Theta_{100})$, where β is equal to peak width at half height [20]. The morphological structures of the ACM were elucidated on a FESEM (Supra PV 55 model).

2.3 Electrochemical characterization

The performance of the supercapacitor cells was studied by a galvanostatic charge-discharge, EIS and cyclic voltammetry using a Solatron 1286 electrochemical interface. The specific capacitance was determined using the formula $C_{sp} = 2C/m$, where C is the cell capacitance and m is the weight of one of the electrodes [21]. The capacitance value of the cell for each measurement method was determined using the following formulas: $C = (I \times \Delta t)/\Delta V$ for galvanostatic charge-discharge, $C = I/s$ for cyclic voltammetry and $C = (2\pi f Z'')^{-1}$ for EIS techniques [22]. I, Δt, ΔV, s, f and Z" represent the constant current, discharge time, voltage, scan rate, frequency and imaginary impedance, respectively. All the measurements were carried out at room temperature (25 ^{o}C).

3. RESULTS AND DISCUSSION

3.1 Physical properties

We successfully prepared several ACMs with highly porous characteristics by a multi-step activation process.

Tabel 2. Weight (W), thickness (t), diameter (D) and density (ρ) of the ACMs with different activation times.

Sample	W	t	D	ρ
	(g)	(mm)	(mm)	(g cm^{-3})
ACM1	0.253	1.642	15.861	0.780
ACM2	0.203	1.657	15.725	0.699
ACM3	0.213	1.646	15.674	0.672
ACM4	0.192	1.599	15.503	0.637
ACM5	0.179	1.629	15.519	0.587
ACM6	0.192	1.599	15.503	0.636

The weight, thickness, diameter and density of the ACMs prepared with different activation times are shown in Table 2. As seen in the table, the weight, diameter and density of the ACMs decrease with increasing activation time. The decrease in the density occurred because the weight loss

was greater than dimensional shrinkage of the samples with increasing activation time. In other words, sample thickness did not decrease at the same rate as weight loss during activation, which may be due to the stacking arrangement of the samples in a vertically positioned tube and their exposure to the flow of CO_2 gas, which comes from the upper side of the tube. Thus, the rounded side surface of the ACMs was more likely to react with the CO_2 gas, which can cause a greater reduction in diameter.

To test the effect of activation time on ACM porosity, the N_2 adsorption-desorption isotherm of ACM2 and ACM4 was observed and is shown in Figure 1. Based on IUPAC data classification, the isotherm profiles for samples ACM2 and ACM4 exhibited a type-IV pattern [23], which represents a combination of microporous and mesoporous characteristics. For ACM2, the volume of adsorbed nitrogen was relatively low. The transition from the critical adsorption at a relatively low pressure to the saturated stages shows a sharp knee, indicating that AMC2 had a narrow pore size distribution. In contrast, ACM4, which was activated at a longer activation time, shows a different adsorption profile. At the lower pressure, the profile had a more rounded knee, while at a higher pressure, there was a gradual increase in adsorption with increasing pressure. These results suggest that samples with longer activation times feature a much wider and more heterogeneous microporosity [24].
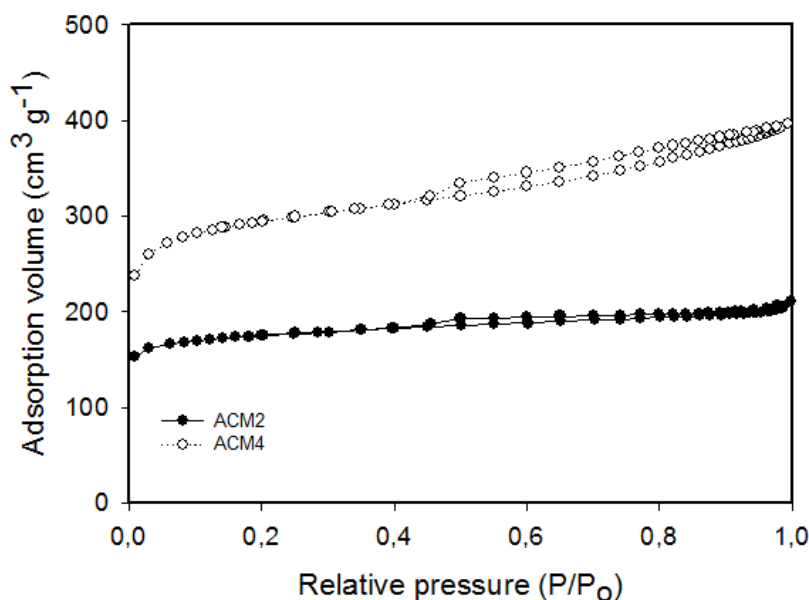

Figure 1. Nitrogen adsorption-desorption isotherms of ACM2 and ACM4 activated for 2 and 4 hours, respectively.

The influence of the multi-step activation process on the improvement of porosity characteristics is also seen in the BET specific surface area (S_{BET}) of the samples listed in Table 3. It can be clearly observed that an increase in activation time from 2 to 4 hours caused nearly a 100% increase in sample surface area due to the development of pores in the samples during activation. With these longer activation times, however, these pores are likely to be deformed [25] from the enlargement of the micropores and the deterioration of the wall between adjacent pores. Hence, this deformation of pores increases the average pore diameter of the carbon. Porosity deformation could

also be a result of an external ablation of the carbon particles, which, in turn, widens the micropores. Based on these results, it can be concluded that activation time plays a significant role in the development of porous structures in the carbon monolith. In addition, ACM6 had a lower specific capacitance compared to ACM4 and ACM5, which is likely due to the deformation of the micropores in ACM6.

Tabel 3. BET surface area (S_{BET}), micropore surface area (S_{mic}), external surface area (S_{ex}), micropore volume (V_{mic}), total pore volume (V_t) and average pore diameter (a) of ACMs with 2 and 4 hours of activation time.

Sample	S_{BET} $(m^2\,g^{-1})$	S_{mic} $(m^2\,g^{-1})$	S_{ex} $(m^2\,g^{-1})$	V_{mic} $(cm^3 g^{-1})$	V_t $(cm^3 g^{-1})$	a (nm)
ACM2	534	414	120	0.21	0.32	2.36
ACM4	913	630	283	0.33	0.61	2.68

Figure 2 shows the FESEM micrographs for the samples with two different lengths of activation time, ACM2 and ACM4. These micrographs clearly show that ACM4 is more porous than ACM2, which has evenly distributed pores with high density. This difference further supports the hypothesis that activation time is instrumental in the formation of the pore network or porous matrix in the ACM derived from RWSD.
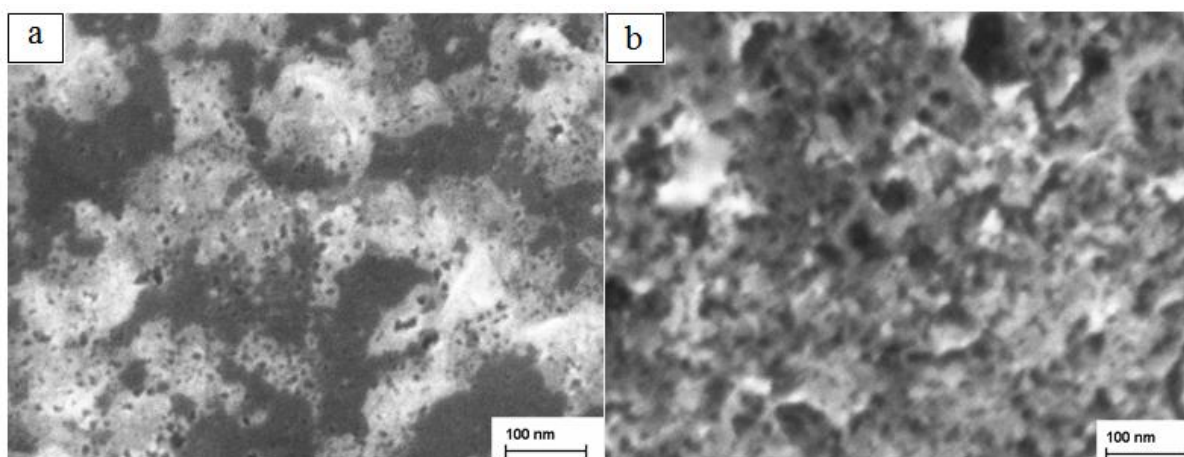

Figure 2. FESEM micrographs of ACM2 and ACM4 activated for 2 (a) and 4 (b) hours, respectively.

Figure 3 shows the XRD patterns of the ACM2 and ACM4 electrodes. Broad peaks corresponding to (002) and (100) planes of the carbon structure appear in both XRD patterns between 15 and 35o. The sharp peaks that appear on the broad peaks are due to the presence of SiO_2 in the electrode, which is commonly found in the biomass raw material. The increase in activation time from 2 to 4 hours resulted in the peaks corresponding to 2Ө at 23.981 and 44.597o for ACM2 shifting to

24.423 and 45.520o for ACM4, respectively. This shift is due to the decrease in the interlayer spacing, d_{002}, from 0.371 to 0.364 nm and in d_{100} from 0.203 to 0.199 nm. The former spacing is in agreement with a previously reported trend [26]. Furthermore, the values of L_c and L_a calculated from these peaks also changed with the increase in activation time. The values of L_c and L_a were 1.147 and 2.286 nm for ACM2 and 0.856 and 2.168 nm for ACM4, respectively, indicating a decrease in the dimension of the graphitic crystallites. This trend is also consistent with that previously reported in the literature [26].
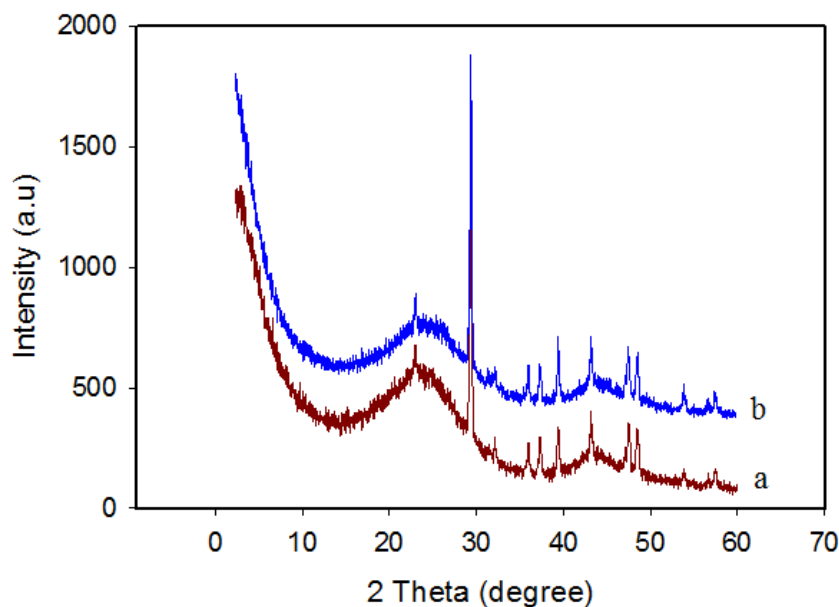

Figure 3. XRD patterns of ACM2 and ACM4 activated for 2 (a) and 4 (b) hours, respectively.

3.2 Electrochemical properties

3.2.1 Electrochemical impedance spectroscopy

EIS is a well-known technique used to study the frequency-dependent behavior of the supercapacitive properties of carbon electrodes. We used the schematic impedance pattern (Nyquist plot) to analyze our data, shown in Figure 4a [27]. In this figure, R_s represents the resistance of the electrolyte and interfacial resistance between the current collector and electrodes. R_p is the intrinsic resistance of the electrodes, and R_f is the equivalent series resistance of the distributed pore resistance in the electrodes.

Figure 4b presents the EIS spectra in the form of Nyquist plots for all of the supercapacitor cells comprising the ACM1 to ACM6 electrodes. Measurements of these spectra were taken at frequencies ranging from 50 kHz to 10 mHz at open circuit potential with an AC perturbation of 10 mV. The values of R_s of the cells with ACM1 to ACM6, estimated from Figure 4b, are listed in Table 4. The values of R_s were almost the same for all of the samples, approximately 0.5 Ohm. This result was expected because all of the cells employed the same electrolyte (H_2SO_4) and they were subjected to the same fabrication method.

From the magnified EIS spectra of the cells (Figure 4b-inset), it can be seen that all show a semicircular pattern in the higher frequency region. The diameters of these semicircles, listed in Table 3, increase with the activation time and indicate the increase in internal resistance of the porous electrode. This change is related to the decrease in density of the porous electrodes during the activation process, which lowers the conductivity of the electrode material. With an increased activation time, the porous matrix would be better developed [28] in the electrode material, which in turn increases its supercapacitive behavior.

Tabel 4. Electrolyte and contact resistance (R_s), intrinsic resistance (R_p) and equivalent series resistance (R_f) of the ACMs with different activation times.

Symmetrical capacitor cells with :	R_s (Ohm)	R_p (Ohm)	R_f (Ohm)
ACM1	0.55	0.75	0.19
ACM2	0.53	0.67	0.13
ACM3	0.54	0.66	0.11
ACM4	0.49	0.80	0.30
ACM5	0.48	0.98	0.49
ACM6	0.52	1.38	0.85

The plots in Figure 4b also show the presence of the Warburg line in the middle frequency range with a slope of approximately 45°. This is an evidence of good diffusion of ions into the bulk of the electrodes porous matrix [27]. At the lower frequency range (i.e., the end of the Warburg line), a line appears (imaginary impedance) with a slope approaching vertical, which represents a capacitive behavior in the electrode materials. This behavior differs for different electrodes with different activation times. The ACM4 and ACM5 cells seem to offer better capacitive behavior compared to the other cells because their imaginary lines lean more toward the imaginary axis.

We can write the following equations for the capacitance, $C(\omega)$, and its real (C') and imaginary (C'') parts [29]:

$$C(\omega) = C'(\omega) - jC''(\omega) \tag{1}$$

$C'(\omega)$ and $C''(\omega)$ are related to the impedance data ($Z(\omega)$) by the following:

$$C'(\omega) = -Z'(\omega)/\omega |Z(\omega)|^2 \tag{2}$$

$$C'' = Z''(\omega)/\omega |Z(\omega)|^2 \tag{3}$$

where

$$Z(\omega) = 1/jC(\omega) \tag{4}$$

Figure 4c presents the variation in the real part of the capacitance (C') with frequency for the ACM1 to ACM6 cells calculated using equation (2).
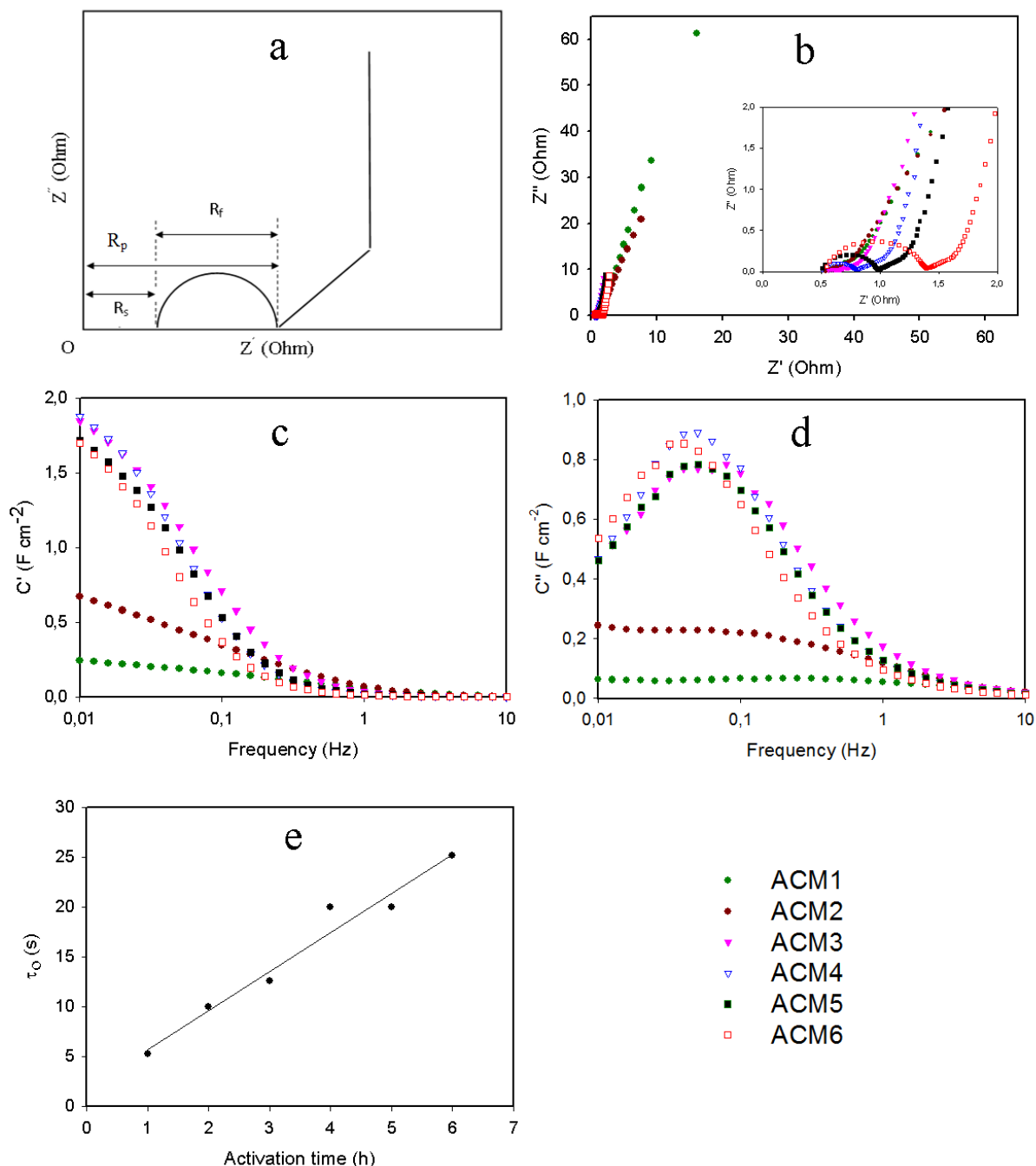

Figure 4. (a) Schematic Nyquist plot, (b) Nyquist plots from 50 kHz to 10 mHz for ACM electrodes of different activation times (inset Nyquis plots from 50 to 1 kHz). Evolution of the real part (c) and the imaginary part (d) of the capacitance versus frequency curve with activation time. (e) The time constant versus activation time.

The C' values for ACM1 and ACM2 are significantly lower in the low frequency region and exhibit a weak frequency dependence compared to the ACM3 to ACM6 cells. In the higher frequency region, the C' values show less frequency dependence and gradually overlap, exhibiting a pure resistive behavior for all the capacitor cells. This result clearly indicates that the optimum activation time lies between 3 and 6 hours. Within this duration, the porous structure of the electrode displays good supercapacitor behavior.

The imaginary part of the capacitance (C") calculated using equation (3) for all of the cells are plotted in Figure 4d as a function of frequency. As in the case of C' (Figure 4c), the values of C" are small and exhibit a weak frequency dependence in the low frequency region for ACM1 and ACM2, whereas the C" values are higher for ACM3 to ACM6 and exhibit a strong frequency dependence with sharp peaks appearing at $f = f_p$. These peaks clearly show that the f_p for ACM6 is slightly lower than those of ACM3 to ACM5, whose f_p values are similar. From these f_p values, one can estimate the relaxation time constant, $\tau_o = 1/f_p$. This constant defines the frontier between the capacitive and resistive behaviors of the supercapacitor. The calculated τ_o values for all of the cells are plotted against activation time in Figure 4e. It is well known that lower τ_o values correspond to higher power delivery [30]. In the present studies, the comparative τ_o values suggest that the ACM3 electrodes are the optimum material for higher power delivery. The 3 hours activation time is enough to develop the porous matrix in the electrode, which exhibited excellent supercapacitive behavior in the low frequency range.

3.2.2 Galvanostatic charge-discharge studies

The constant current charge-discharge studies of the supercapacitor cell were performed between cell voltages of 0.01 and 1.0 V at two different discharge current densities of 10 and 30 mA cm^{-2}, as shown in Figure 5a and 5b, respectively.
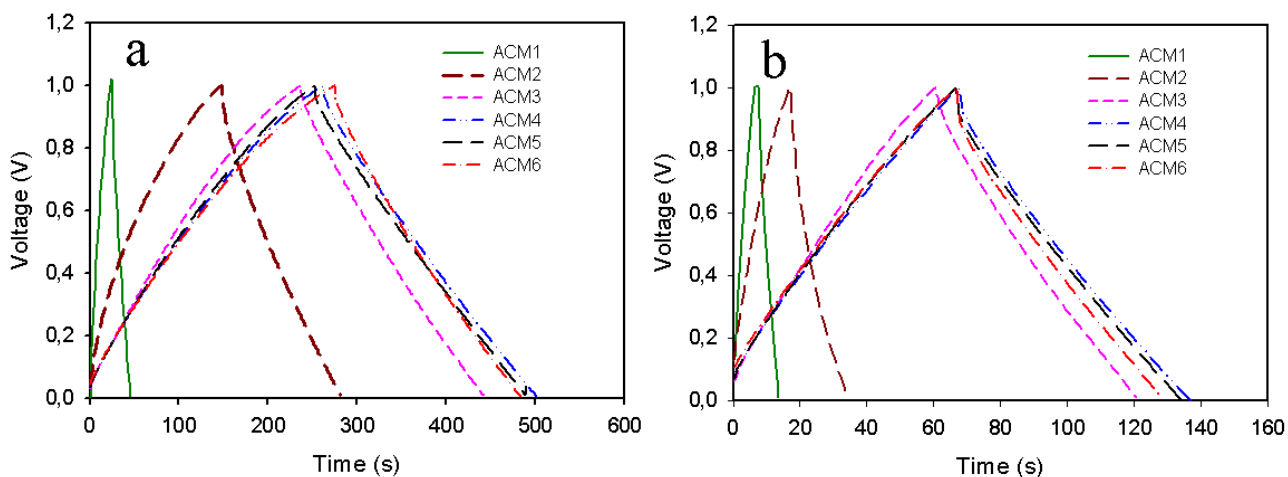

Figure 5. Potential-time curves of ACM electrodes with different activation times obtained at current densities of (a) 10 mA/cm^2 and (b) 30 mA/cm^2.

All the charge-discharge curves had a similar shape, which is a typical pattern for carbon electrode-based cells with capacitive behavior [31]. The supercapacitors based on ACM1 and ACM2 had shorter discharge times than the ACM3- to ACM6-based cells. The ACM5 cell had the longest discharge time. Additionally, there was a sudden potential drop during the initial discharge for each cell. Such potential drops were relatively small, indicating that the supercapacitor cells had a low series resistance value that is attributable to the good conductivity and mesoporous nature of these CO_2-activated carbon electrodes.

3.2.3 Cyclic voltammetry

The cyclic voltammograms of the supercapacitor cells based on the carbon electrodes ACM1 to ACM6 are shown in Figure 6 for the potential window from 0 to 1 V with a scan rate of 1 mV s^{-1}. All cells had similar rectangular-like shapes without any redox current peaks on both the positive and negative sweeps in the potential range of investigation. The voltammetric charges on the positive and negative sweeps were approximately equal for all curves, which demonstrates that the charge-discharge behavior of these ACMs in H_2SO_4 was highly reversible, further indicating that the electrodes have good capacitive behavior [32]. An increase in activation time led to an increase in the current values of the voltammograms. This is a consequence of the increase both in surface area with increasing activation time and in the accessibility of electrolytes to the porous matrix of electrodes.
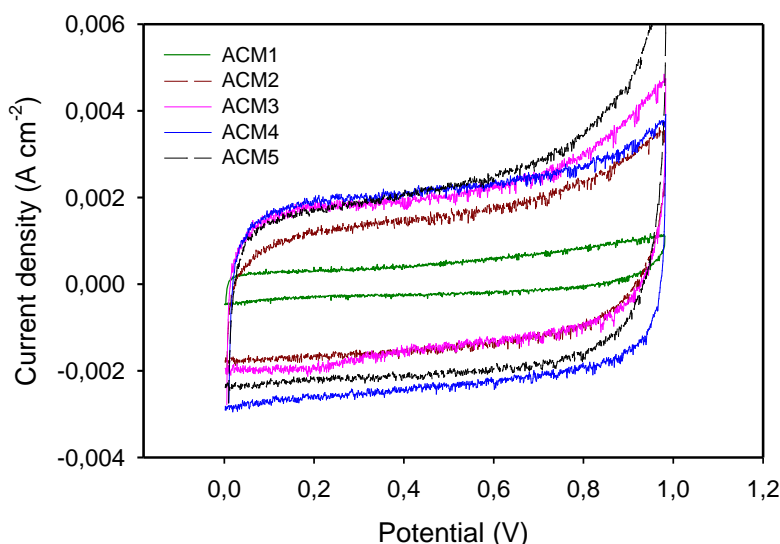

Figure 6. Cyclic voltammograms of ACM electrodes with different activation times obtained at a scan rate of 1 mV s^{-1}.

3.3 Comparison of specific capacitance

Comparative values of specific capacitance from all three methods (galvanostatic charge-discharge, cyclic voltammetry and EIS) for all the electrodes are listed in Table 5. From each method

of measurement, a general trend of increasing specific capacitance with increasing activation time was observed, with the maximum value for ACM5 (5-hour activation time). Increasing the activation time past 5 hours decreased the specific capacitance (Table 5). These results demonstrate that the specific capacitance obtained from the three different independent techniques are in good agreement and exhibit a similar trend of change with changing activation time. Similar agreement has also been reported for resorcinol-formaldehyde-based porous carbon electrodes [33].

Tabel 5. Specific capacitance obtained from constant current charge-discharge (GC), EIS and cyclic voltammetry methods.

Symmetrical capacitors cell :	Csp (GC 0.01 A cm^{-2}) (F g^{-1})	Csp (GC 0.03 A cm^{-2}) (F g^{-1})	Csp (EIS) (F g^{-1})	Csp CV (F g^{-1})
ACM1	7.86	7.64	9.02	13.33
ACM2	51.00	21.30	28.37	54.31
ACM3	90.10	79.94	85.84	73.32
ACM4	107.64	95.33	92.17	105.36
ACM5	138.71	121.58	105.49	121.42
ACM6	101.41	96.23	96.23	-

There are many reports in the literature describing supercapacitors fabricated with carbon electrodes prepared from different biomass precursors [3-10, 34]. A comparative list of specific capacitance values from these different electrodes, including the present study, is summarized in Table 6 along with their BET specific surface areas. These comparative data show that our results are within the typical range reported by other researchers, indicating that the method of carbon electrode preparation proposed in the present study is satisfactory.

Tabel 6. Electrodes of supercapacitors from biomass precursors.

Biomass Precursor	Specific Capacitance (F g^{-1})	BET Surface Area (m^2 g^{-1})	Reference
Cassava peel	153	1352	[3]
Coffee beans waste	368	1029	[4]
Coffee shells	150	842	[5]
Cherry stones	232	1292	[6]
Bamboo	68	1251	[7]
Fir wood	197	2821	[8]
Banana fiber	74	1079	[9]
Sugar cane bagasse	300	1452	[10]
Bamboo	60	1025	[34]
RWSD	138	912	Present Study

3.4 Specific energy and specific powers

The Ragone plots (i.e., specific power versus specific energy) for the supercapacitor cells with ACM1 to ACM6 electrodes are shown in Figure 7 The energy and power relationship of this plot was calculated by applying the formulas $E = Vit/m$ and $P = Vi/m$, respectively where i is discharge current, V is voltage excluding the iR drop occuring at the beginning of the discharge, t is time in hour and m is the mass [35] from the charge and discharge curves at a current density of 30 mA (Figure 5b). A gradual decrease in specific power was observed with increasing specific energy for the cells employing the ACM3 to ACM6 electrodes. The ACM1 and ACM2 cells offer a fast decrease in specific power versus specific energy. The maximum energy density was produced by the ACM5 cell with a value of 2.63 Wh kg-1 at a power density of 291 W kg-1. These results fall within the typical range of specific energy and specific power density for supercapacitors [36].
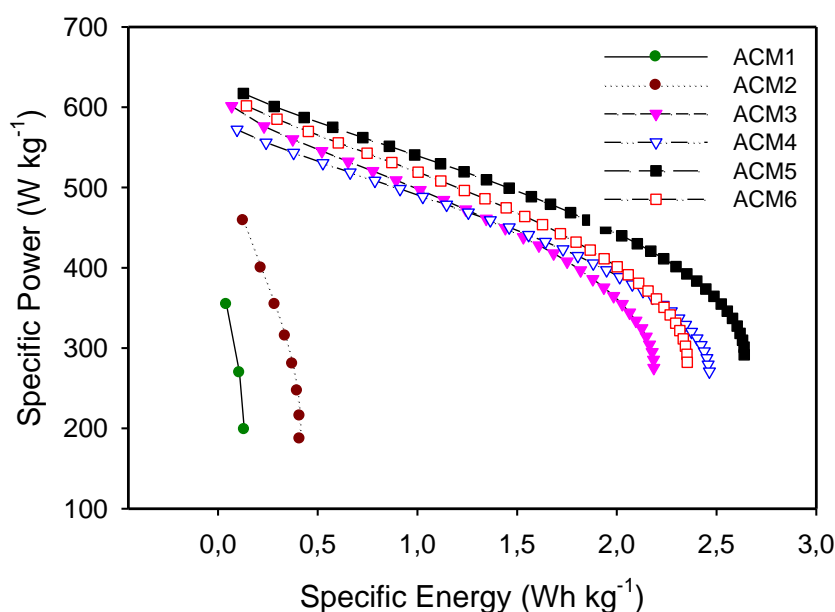

Figure 7. Specific power versus specific energy for ACM electrodes of different activation times.

4. CONCLUSIONS

Binderless porous ACMs for use as supercapacitor electrodes were prepared from the self-adhesive carbon grains of RWSD. A multi-step CO_2 activation process was used for their preparation with different activation times (i.e., 1, 2, 3, 4, 5 and 6 hours) to optimize their porosity. The absence of binder is advantageous because it lowers equivalent series resistance. Multi-step activation is necessary to ensure that the monoliths are free of cracks. A longer activation time (approximately 5 hours) produced lower density, smaller graphitic microcrystallite dimensions and a porous electrode structure with micro- and mesoporosity. These results show how an improved pore network and higher surface area were obtained, which enhances supercapacitive behavior. The optimum activation time was found

to be 5 hours, yielding a specific capacitance of 138 F g^{-1}, a specific energy of 2.63 Wh kg^{-1} and a specific power of 291 W kg^{-1}. Thus, the combined roles of multi-step activation and optimum activation time produced a good quality binderless ACMs from RWSD for supercapacitor electrodes.

References

1. R. Kotz, M. Carlen, *Electrochim Acta.* 45 (2000) 2483.
2. E. Frackowiak, F. Beguin, *Carbon.* 39 (2001) 937.
3. A.E. Ismanto, S.Wang, F.E. Soetaredjo, S. Ismadji, *Bioresource Technol.* 101 (2010) 3534.
4. T.E. Rufford, D. Hulicova-Jurcakova, Z. Zhu, G.Q. Lu, *Electrochem Comm.* 10 (2008) 1594.
5. M.R. Jisha, Y.J. Hwang, J.S. Shin, K.S. Nahm, T.P. Kumar, K. Karthikeyan, N.Dhanikaivelu, D.Kalpana, N.G. Reganathan, A.M. Stephan, *Mater Chem and Phys*. 115 (2009) 33.
6. M. Olivares-Marin, J.A. Fernandez, M.J. Lazaro, C. Fernandez-Gonzalez, A. Marcias-Garcia, V. Gomez-Serrano, et al, *Mater Chem and Phys*. 114 (2009) 323.
7. Y.J. Kim, B-J. Lee, H. Suezaki, T. Chino, Y. Abe, T. Yanagiura, K. C. Park, M. Endo, *Carbon*. 44 (2006) 1581.
8. F-C.Wu, R-L.Tseng, C-C.Hu, C-C.Wang, *J Power Sources.* 159 (2006) 1532.
9. V.Subramaniam, C.Luo, A.M. Stephan, K.S. Nahm, S.Thomas, B.Wei, *J. Phys. Chem. C*. 111 (2007) 7527.
10. T.E. Rufford, D.Hulicova-Jurcakova, K. Khosla, Z. Zhu, G.Q. Lu, *J Powers Sources*. 193 (2010) 912.
11. V. Ruiz, C. Blanco, R. Santamaria, J.M. Ramos-Fernandez, M. Martinez-Escandell, Sepulveda-Escribano A, F. Rodriquez-Reinoso, *Carbon*. 47 (2009) 195.
12. A.Garcia-Gomez, P. Miles, T.A. Centeno, J.M. Rojo, *Electrochim Acta*. 55 (2010) 8539.
13. J.M.V. Nabais, J.G. Teixeira, I. Almeida, *Bioresource Technol*. 102 (2011) 2781.
14. V. Ruiz, C. Blanco, M. Granda, R. Menendez, *J Appl Electrochem.* 37 (2007) 717.
15. T.C. Weng, H. Teng, *J Electrochem Soc*. 148 (2001) 368.
16. A.R. Mohamed, M. Mohammadi, G.N. Darzi, *J Renew Sustain Energy Rev*. 14 (2010) 1591.
17. E. Taer, M. Deraman, I.A. Talib, A.A. Umar, M. Oyama, R.M. Yunus, *Cur Appl Phys*. 10 (2010) 1071.
18. M. Deraman, R. Omar, S. Zakari, I.R. Mustapa, M. Talib, N. Alias, *J Mater Sci*. 37 (2002) 3329.
19. P.A. Webb, Orr C. Analytical methods in fine particle technology. Norcross: Georgia, USA, Micromeritiecs Instrument Corp (1997).
20. P.J.M. Carrott, J.M.V. Nabais, M.M.L. Ribeiro Carrott, J.A, *Carbon.* 39 (2001) 1543.
21. C. Portet, P.L. Taberna, P. Simon, E. Flahaut, C. Laberty-Robert, *Electrochim Acta*. 50 (2005) 4174.
22. Y. Zhu, H. Hu, W. Li, X. Zhang, *Carbon.* 45 (2007) 160.
23. K.S.W. Sing, D.H. Everret, R.A.W. Haul, L. Moscou, R.A. Pierotti, J. Rouquerol, T. Siemieniewska, *Pure Appl. Chem.* 57 (1985) 603.
24. S. Guo, J. Peng, W. Li, K. Yang, L. Zhang, S. Zhang, at al, *Appl Surface Sci.* 255 (2009) 8443.
25. P.J.M. Carrott, *Carbon*. 29 (1991) 499.
26. X. He, J. Lei, Y. Geng, X. Zhang, M. Wu, M. Zheng, *J Phys and Chem of Solids*. 70 (2009) 738.

27. X-M. Liu, R. Zhang, L. Zhan, D-H. Long, W-M. Qiao, J-H. Yang, L.-C. Ling, *New Carbon Mater.* 22 (2007) 153.
28. J. Gambia, P.L. Taberna, P. Simon, J.F. Fauvarque, M. Chesneau, *J Power Sources.* 101 (2001) 109.
29. J. Chimiola, G. Yushin, R. Dash, Y.Gogotsi, *J Power Sources.* 158 (2006) 765.
30. D. Pech, M. Brunet, H. Duron, P. Huang, V. Mochalin, Y. Gogotsi, P.-L. Taberna, P. Simon, *Nature Nanotech.* 162 (2010) 651.
31. M.S. Michael, S.R.S. Prabaharan, *J Power Sources.* 136 (2004) 250.
32. S-I. Lee, S. Mitani, C.W. Park, S-H. Yoon, Y. Korai, I. Mochida, *J Power Sources.* 139 (2005) 379.
33. Y. Zhu, H. Hu, W. Li, X. Zhang, *Carbon.* 45 (2007) 160.
34. C. Kim, J-W. Lee, J-H. Kim, K-S. Yang, *Korean J Chem Eng.* 23 (2006) 592.
35. S.R.S. Prabahan, R. Vimala, Z. Zainal, *J Power Sources.* 161 (2006) 730.
36. P. Simon, Y. Gogotsi, *Nature Mater.* 7 (2008) 845.